Quadratic band touching with long-range interactions in and out of equilibrium

Balázs Dóra[1,*] and Igor F. Herbut[2]

[1]*Department of Theoretical Physics and MTA-BME Lendület Spintronics Research Group (PROSPIN), Budapest University of Technology and Economics, Budafoki út 8, 1111 Budapest, Hungary*

[2]*Department of Physics, Simon Fraser University, Burnaby, British Columbia, Canada V5A 1S6*

(Received 3 June 2016; revised manuscript received 26 September 2016; published 20 October 2016)

Motivated by recent advances in cold atomic systems, we study the equilibrium and quench properties of two-dimensional fermions with quadratic band touching at the Fermi level, in the presence of infinitely long-range interactions. Unlike when only short-range interactions are present, both nematic and quantum anomalous Hall (QAH) states appear at weak interactions, separated by a narrow coexistence region, whose boundaries mark second- and third-order quantum phase transitions. After an interaction quench, the QAH order exhibits three distinct regions: persistent or damped oscillations and exponential decay to zero. In contrast, the nematic order *always* reaches a nonzero stationary value through power-law damped oscillations, due to the interplay between the symmetry of the interaction and the specific topology of the quadratic band touching.

DOI: 10.1103/PhysRevB.94.155134

I. INTRODUCTION

Quantum quenches and nonequilibrium dynamics are penetrating into many fields of physics, including condensed matter, cold atoms, high-energy physics, mesoscopic systems, etc. [1,2]. Considering the nonequilibrium time evolution, not only can one address fundamental questions related to equilibration and thermalization, but reaching novel states of matter without an equilibrium counterpart [3,4], such as Floquet topological systems without an external drive [5], also becomes possible.

Strongly correlated systems with short-range interactions contain plenty of rich physics, in spite of being notoriously difficult to deal with in dimensions higher than one, especially when driven out of equilibrium after a quantum quench. Mean-field models, on the other hand, while easily solvable, neglect the interesting physics of quantum fluctuations. Models with long-range interactions bridge between them and combine the best of the two by containing interaction terms, and yet being exactly solvable in any dimension, at least in the thermodynamic limit. Such models belong to the family of Richardson-Gaudin models [6,7].

The Richardson-Gaudin models models are characterized by infinitely long, global range interactions. Consequently, the Mermin-Wagner theorem is not applicable and ordering can take place independently of the dimensionality of the problem. These models thus constitute the extreme opposite limit of short-range interactions. It seems also plausible that interacting models with power-law interactions [8,9] may lead to phases and phase transition characteristics of either short-range or infinite-range interacting models, which adds to the importance of Richardson-Gaudin type models. Last but not least, fermionic systems with infinitely long-range interactions have recently been realized in cold atomic systems. In cavity QED, a single cavity mode in an optical resonator interacting with fermions can be eliminated [10–13] to yield an effective Hamiltonian that describes the long-range atom-atom interaction. An alternative method includes trapped ions interacting with lasers [14,15].

Quantum quenches in Richardson-Gaudin models have been studied by focusing on the fate of a superconducting state upon an abrupt change (i.e., quantum quench) of the interaction parameter [16–20]. The ensuing dynamics is expected to be universal due to the long relaxation time in cold atomic systems, where such experiments were conducted. This approach was also extended to the presence of multiple, *fully gapped* order parameters developing on top of topologically *trivial* noninteracting band structures [21–23].

Our goal here is to add another twist to the story by considering time evolution in the presence of long-range repulsive interactions around a quadratic band touching (QBT) crossing point, carrying a Berry phase of 2π. Such systems have been intensively studied in equilibrium and in the presence of short-range interactions [24–27] that yield a topologically ordered, quantum anomalous Hall state (QAH) [28], which typically wins over the nematic phase. We find, in contrast, that the nematic state competes successfully against the QAH in the presence of long-range interactions, and actually becomes more robust against quantum quenches than QAH. We attribute the latter feature to the specific topology of the noninteracting dispersion.

II. MODEL

The spinless model we focus on is the generalization of that in Ref. [24] in the presence of long-range interactions. The kinetic energy in the second quantized form is

$$H_0 = \sum_{\mathbf{p}} \epsilon_{\mathbf{p}} \left[\cos(2\varphi_p) S^x_{\mathbf{p}} + \sin(2\varphi_p) S^y_{\mathbf{p}} \right], \tag{1}$$

where $\epsilon_{\mathbf{p}} = p^2/2m, m > 0$ is the effective mass, and p and φ_p are the radial and angular coordinates in two dimensions (2D). $S^i_{\mathbf{p}} = \Psi^+_{\mathbf{p}} \sigma_i \Psi_{\mathbf{p}}$ is a pseudospin operator acting in the particle-hole channel, and is analogous to Anderson's pseudospin operator [29]. We have defined $\Psi^+_{\mathbf{p}} = (a^+_{\mathbf{p}}, b^+_{\mathbf{p}})$, σ's are Pauli matrices, and $a^+_{\mathbf{p}}$ and $b^+_{\mathbf{p}}$ are creation operators of electrons with momentum $\mathbf{p}$ on two distinct sublattices [24,25,27]. The resulting noninteracting spectrum describes a QBT at $p = 0$

*dora@eik.bme.hu

as $\pm\epsilon_{\mathbf{p}}$ and is characterized by a nontrivial Berry phase of 2π [30].

The infinitely long-range interactions (both in real and momentum space; see the Appendix) between the pseudospins is

$$H_{\rm int} = -\sum_{i=x,y,z} \frac{g_i}{4N} \left(\sum_{\mathbf{p}} S^i_{\mathbf{p}} \right)^2, \tag{2}$$

where N is the number of unit cells in the system. Similar interactions involving the sublattice degrees of freedom have already been engineered in Ref. [13]. This interaction represents the long-range generalization of Ref. [24]. Due to the long-range nature of the interaction, distinct coupling constants are possible for the different pseudospin components, in contrast to the case of short-range interactions, which allows only one, marginally relevant, coupling constant. Each pseudospin interacts with all others in the momentum space, so that the number of nearest-neighbor pseudospin components in momentum space is infinity. This way, the self-consistent mean-field theory becomes exact in the thermodynamic limit.

In this limit, the instabilities manifest themselves as finite expectation values of the pseudospin operators. In particular, similarly to the case of short-range interactions, a finite $\langle S^z \rangle = \sum_{\mathbf{p}} \langle S^z_{\mathbf{p}} \rangle / N$ order parameter breaks a discrete symmetry, gaps out the full spectrum, and yields the quantum anomalous Hall order. A state with a finite QAH order parameter is topologically nontrivial, and yields a quantized Hall response as $\sigma_{xy} = \pm e^2/h$, irrespective of the presence or absence of nematic order. A finite $\langle S^{x,y} \rangle = \sum_{\mathbf{p}} \langle S^{x,y}_{\mathbf{p}} \rangle / N$ corresponds to nematic order, and breaks the continuous $U(1)$ rotational symmetry of the spectrum by splitting the quadratic band crossing into two linearly dispersing Dirac cones at finite momentum, each carrying a Berry phase of π.

In principle, due to its structure, our model belongs to the family of Richardson-Gaudin models. For arbitrary interactions, however, it cannot be mapped to an effective one-dimensional problem of the Richardson-Gaudin type, and to the best of our knowledge, no exact solution is known for it. This is because the φ_p appears in the kinetic energy part, and can only be eliminated by a rotation around S^z, which would then modify the nematic part of the interaction.

III. EQUILIBRIUM PHASE DIAGRAM

The physical order parameters appear also in the spectrum through $\Delta = g^z \sum_{\mathbf{p}} \langle S^z_{\mathbf{p}} \rangle / 2N$ and $m_{x,y} = g^{x,y} \sum_{\mathbf{p}} \langle S^{x,y}_{\mathbf{p}} \rangle / 2N$. The zero temperature ground-state energy of the system contains the energy gain due to opening of the gaps and the elastic terms as

$$E_0 = -\rho \int_0^W d\epsilon \int_0^\pi \frac{d\phi}{\pi} \tilde{\epsilon} + \frac{\Delta^2}{g_z} + \frac{m_x^2}{g_x}, \tag{3}$$

with $\tilde{\epsilon} = \sqrt{\epsilon^2 + \Delta^2 + m_x^2 - 2\epsilon m_x \cos(\phi)}$, $\rho = m/2\pi$ is the density of states, and W is the high-energy cutoff. The order parameters are obtained by minimizing it. For the sake of simplicity, we assume that nematic order develops in the x direction. The gap equations are

$$[\Delta, m_x] = \rho \int_0^W d\epsilon \int_0^\pi \frac{d\phi}{\pi} \frac{[g_z\Delta, g_x(m_x - \epsilon\cos(\phi))]}{2\tilde{\epsilon}}. \tag{4}$$

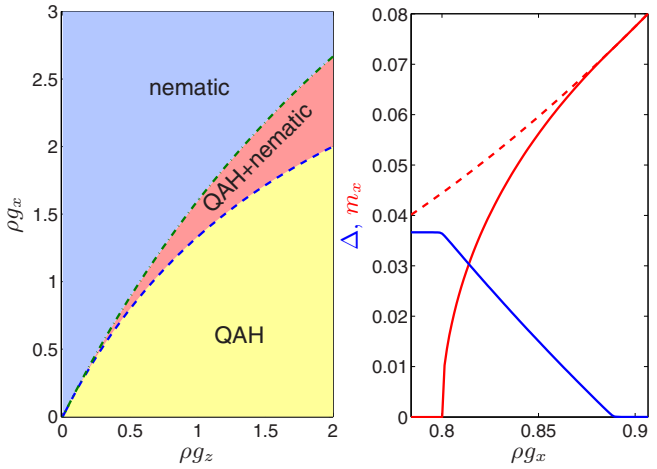

FIG. 1. The weak-coupling phase diagram of Eqs. (1) and (2) for $g_x \gtrless g_y$ in the weak-coupling limit is shown in the left panel. For $g_y > g_x$, g_x should be replaced by g_y. The blue dashed/green dashed-dotted lines denote a second/topological third-order transition, respectively. Right panel: Nematic (red) and QAH (blue) order parameters are shown for $\rho g_z = \frac{1}{2}$ in the coexisting region. The red dashed line denotes the nematic gap without QAH, which is only a local minimum of the ground-state energy compared to the coexisting solution.

Using a full lattice model would not alter our results qualitatively. For $g_x = g_y$, the angle of the order parameter remains undetermined from the mean-field equations, and becomes the Goldstone mode of the continuous rotational symmetry breaking. For $g_x \gtrless g_y$, the bare interaction itself breaks the rotational symmetry and nematic order, breaking now a discrete Z_2 symmetry, develops only in the x/y direction, respectively.

The phase diagram emerging from Eqs. (4) is shown in Fig. 1, which is our first important result. For $g_z \gg g_x$, the QAH phase suppresses nematic order, while in the opposite, $g_x \gg g_z$ situation, the nematic order wins. In between, two phase boundaries are identified, corresponding to continuous phase transitions. The $g_x = 4g_z/(2 + \rho g_z)$ line in the weak-coupling limit marks a second-order transition according to Ehrenfest classification and separates the pure QAH state from a coexisting QAH and nematic phase. The nematic order parameter rises as $m_x \sim \sqrt{|g - g_c|}$, and the ground-state energy changes as $E_0 \sim m_x^4$, so that its second derivative is discontinuous.

The $g_x = 8g_z/(4 + \rho g_z)$ weak-coupling line, on the other hand, denotes a topological, third-order transition from the phase with coexisting orders to a pure nematic state. The QAH order varies as $\Delta \sim |g - g_c|$, producing $E_0 \sim \Delta^3$ with a jump in the third derivative. The third-order transition is characteristic of the mean-field Dirac metal-insulator transition, as noted already in Ref. [31]. A third-order topological transition occurs also in the related long-range interacting model [7]. It is an interesting feature of our model that not only nematic order appears in the weak-coupling limit, but it also coexists

with QAH for vanishingly small couplings, in sharp contrast to the case of short-range interactions [24]. In the noncoexisting regions, the conventional weak-coupling forms are recovered as $\Delta = 2W\exp(-2/\rho g_z)$ and $m_x = 4W\exp(\frac{1}{2} - 4/\rho g_x)$.

We note that for models with weak short-range interactions the couplings in the nematic and QAH channels are related to each other, and there is essentially only a single coupling constant. This is the crucial difference in our long-range interacting model, which allows for different and unrelated couplings for distinct ordering channels, e.g., $g_{x,y,z}$. As a result, the QAH always wins over nematic for the short-range case in the weak-coupling limit, and the latter phase can only appear for stronger couplings [24]. The order of the transition is also different in the short-range and the long-range cases, but its further analysis is beyond the scope of our work.

IV. QUANTUM QUENCH

Having determined the equilibrium properties of $H_0 + H_{\rm int}$, we turn to its behavior after an interaction quantum quench. The model initially sits in the ground state for some coupling parameters, which changes abruptly to some other value at $t = 0$. The ensuing dynamics is governed by the time-dependent mean-field theory [16–19], yielding

$$\partial_t S^x_{\mathbf{p}} = 2\epsilon_{\mathbf{p}}\sin(2\varphi_p)S^z_{\mathbf{p}} + g_z S^z(t)S^y_{\mathbf{p}} - g_y S^y(t)S^z_{\mathbf{p}}, \quad (5a)$$

$$\partial_t S^y_{\mathbf{p}} = -2\epsilon_{\mathbf{p}}\cos(2\varphi_p)S^z_{\mathbf{p}} + g_x S^x(t)S^z_{\mathbf{p}} - g_z S^z(t)S^x_{\mathbf{p}}, \quad (5b)$$

$$\partial_t S^z_{\mathbf{p}} = 2\epsilon_{\mathbf{p}}\big[\cos(2\varphi_p)S^y_{\mathbf{p}} - \sin(2\varphi_p)S^x_{\mathbf{p}}\big] + g_y S^y(t)S^x_{\mathbf{p}} - g_x S^x(t)S^y_{\mathbf{p}}, \quad (5c)$$

where $S^i(t) = \sum_{\mathbf{p}}\langle S^i_{\mathbf{p}}\rangle/N$ is the time-evolved order parameter after the quench. The initial conditions at $t = 0$ are

$$\begin{pmatrix}\langle S^x_{\mathbf{p}}\rangle\\ \langle S^y_{\mathbf{p}}\rangle\\ \langle S^z_{\mathbf{p}}\rangle\end{pmatrix} = \begin{pmatrix}m_x - \epsilon_{\mathbf{p}}\cos(2\varphi_p)\\ -\epsilon_{\mathbf{p}}\sin(2\varphi_p)\\ \Delta\end{pmatrix} \times E^{-1}_{\mathbf{p}}, \quad (6)$$

where $E_{\mathbf{p}} = \sqrt{\epsilon^2_{\mathbf{p}} + \Delta^2 + m_x^2 - 2\epsilon_{\mathbf{p}} m_x\cos(2\varphi_p)}$.

Equations (5) are solved numerically using, e.g., a fourth-order Runge-Kutta method. Since the full parameter space is large due to the distinct coupling constants in Eq. (2) before and after quench, we focus on the time evolution of the pure QAH and nematic order parameters, when only their respective coupling constants are present and quenched.

V. QAH QUENCH

In the pure QAH case with $g_{x,y} = 0$, the phase variable φ_p can be transformed away by a rotation around z for each pseudospin, leaving us with an effective one-dimensional model of the Richardson-Gaudin type [6], which depends only on the momentum p, and which is exactly solvable.

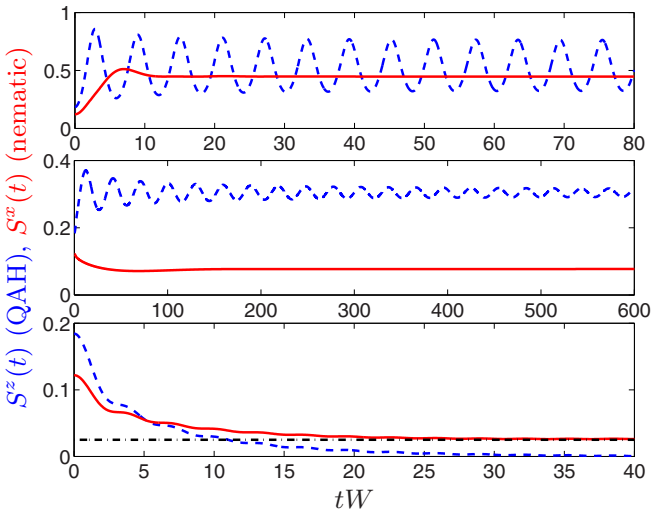

FIG. 2. The time evolution of the QAH (blue dashed) and nematic (red solid) order parameters are shown, starting from $\Delta = 0.05W$ or $m_x = 0.05W$, corresponding to an initial coupling $\rho g_z = 0.543$ or $\rho g_x = 0.819$, respectively, and $\rho W = 1$. After the quench, $\rho g_{z,x} = 2$ (top panel), 0.7 (middle panel), and 0.1 (bottom panel). For the latter, the steady-state value is indicated by a black dashed-dotted from Eq. (8). The tiny oscillation superimposed on the temporal decay arises from a finite cutoff, which is needed to make $S^{x,z}(t = 0)$ finite.

The interaction, however, here is of an "easy axis" type, e.g., $-(S^z)^2$, in contrast to the usual "easy plane" interaction in the BCS theory, which is $-(S^x)^2 - (S^y)^2$. In other words, the QAH order parameter is always real and associated with breaking of a discrete symmetry, whereas the BCS order parameter breaks the continuous $U(1)$ symmetry. Nevertheless, the emerging picture resembles closely that of a quenched BCS superconductor, and reveals three qualitatively distinct regions in the temporal dynamics, as shown in Fig. 2. For large final coupling, persistent, nondecaying oscillations show up in the time dependence, and this phase-locked, self-induced, synchronized oscillation can be used to realize an externally nondriven Floquet topological phase, similarly to p-wave superconductors [5]. For medium values of the final coupling, the QAH order parameter reaches a time-independent steady-state value through power-law decaying ($\sim t^{-1/2}$) damped oscillations, while for small quenches, an exponential decay to zero occurs. Note that tiny additional oscillations of the form $\sin(2Wt)/Wt$ are superimposed on the decay due to the finite cutoff W, which is essential to keep the equilibrium $S^z(t = 0)$ finite. These three regions are separated by dynamical phase transitions [17,32]: The oscillation amplitude and the asymptotic value of the order parameter vanish continuously at the critical points.

VI. NEMATIC QUENCH

The quench of a pure nematic state with $g_{y,z} = 0$, on the other hand, is characterized by completely different behavior. No dynamical phase transition occurs at all, and the time evolution is characterized by damped oscillations with a much faster decay when compared to the QAH case. This is due

to the existence of low-energy excitations around the linearly dispersing Dirac points, as visualized in Fig. 2. The crucial difference with respect to previously considered quenches in superconductors [17,33] occurs, however, for small finite couplings. In this limit, the nematic order parameter does not vanish but approaches a finite, time-independent stationary value. This is best illustrated by completely switching off the nematic coupling, in which case Eqs. (5) admit a simple solution as

$$\langle S^x_{\mathbf{p}}\rangle = \frac{m_x[\cos(2\epsilon_{\mathbf{p}}t)\sin^2(2\varphi_p)+\cos^2(2\varphi_p)]-\epsilon_{\mathbf{p}}\cos(2\varphi_p)}{\sqrt{\epsilon^2_{\mathbf{p}}+m_x^2-2\epsilon_{\mathbf{p}}m_x\cos(2\varphi_p)}}, \tag{7}$$

yielding, after momentum integration, in the stationary state when $t\to\infty$,

$$S^x_{\mathrm{st}} = \frac{\rho m_x}{2}, \tag{8}$$

with the superimposed power-law decay, $\sim\rho\cos(2m_xt)/m_x^2t^3$, obtained through the method of steepest descent. The exponent of the power law differs both from those in s-wave [34] or d-wave [33] superconductors, in spite of the latter also possessing low-energy Dirac-like quasiparticles. This reflects both the linearly dispersing Dirac cones and the nontrivial 2π Berry phase and results in heavily damped oscillations in Fig. 2. Since no qualitative change occurs in the time evolution of the order parameter with increasing final coupling, this supports the idea [19] that both the final stationary value, together with the $\sim t^{-3}$ decay, is a universal feature of the nematic phase.

Equation (8) is our second main result. Its universality (i.e., W independence) implies that it is expected to hold in any lattice model hosting a QBT. It is surprising for several reasons: First, the nematic order is always suppressed for short-range interactions in equilibrium [24], and although it competes with QAH successfully for long-range interactions, it would be naively expected to be more vulnerable to time dependence of the interaction coupling, due to its low-energy excitations. Second, the equilibrium low-energy thermodynamics of 2D Dirac fermions is universal, no matter whether it is for graphene [35], d-wave superconductors [36], or the present nematic state. In sharp contrast, the dynamics after a quench differs significantly from that of a d-wave BCS superconductor [33] where the order parameter vanishes identically for small quenches. We trace this difference back to the nontrivial, noninteracting spectrum and its 2π Berry phase in Eq. (1), as well as to the structure of the interaction, both of which conspire to produce the nematic order. In contrast, d-wave superconductivity is induced only by the symmetry of the interaction [33] and is largely insensitive to the bare dispersion; its stationary state therefore resembles closely that of an s-wave superconductor.

Third, the survival of the nematic order does *not* simply follow from energetics [17], namely, from comparing the postquench energy of the system to that of an equilibrium nematic state, to estimate its effective temperature. For an interaction switch-off in the weak-coupling limit, the energy considerations are identical to that in a d-wave superconductor, where, in contrast to Eq. (8), the order parameter vanishes [33]. In spite of the deduced effective temperature being above the equilibrium critical temperature for the nematic ordering, nematicity survives the quench. The essential difference between nematic and superconducting states lies in the pseudospin structure. An initial pseudospin polarized state in the x-y plane is driven by a pseudomagnetic field in the z direction for a superconductor or by an in-plane hedgehoglike field configuration from H_0 for the nematic state. While the former produces complete dephasing, the latter dephases only partially, and still preserves some information of the initial state.

We also find that starting from an initial coexisting nematic and QAH phase and switching off the interactions, the nematic order survives according to Eq. (8) while the QAH vanishes.

We have so far focused on easy axis nematic quenches with $g_x\neq 0$ and $g_y=g_z=0$, but our results apply equally to easy plane nematic quenches with $g_x>g_y>0$ and $g_z=0$, when only a discrete symmetry is broken in equilibrium by the nematic order and the ground-state energy possesses a discrete number of minima. On the other hand, for $g_x=g_y$, a continuous symmetry is broken, the equilibrium ground-state energy has a sombrero structure, with all of the minima ending up being mixed after a quench. Consequently, the above solution with only $S^x\neq 0$ is unstable with respect to any small $S^{y,z}$ additional order parameters.

VII. STEADY STATE

Based on these, we can construct the stationary state phase diagram of the system, shown in Fig. 3. The stationary values of the nematic and QAH order behave qualitatively similarly, except for small quenches where only the nematic order survives. The phase diagram pertaining to the QAH

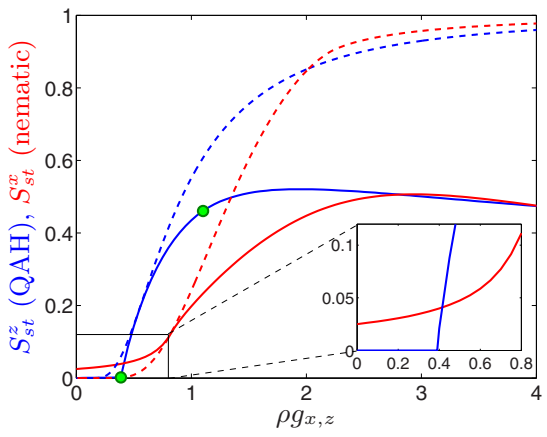

FIG. 3. The steady-state behavior of the order parameter is plotted for the pure QAH (blue) and nematic (red) state, starting from either $\Delta=0.05W$ or $m_x=0.05W$ in the respective channel. The green dots denote the three qualitatively different regions of the QAH order parameter. The dashed lines are the equilibrium order parameters from the solution of Eqs. (4). The inset zooms into the weak-coupling limit.

state features two dynamical transitions at which the time dependence changes qualitatively: The exponential decay to zero for small quenches is replaced by damped and undamped oscillations with increasing final interaction. In contrast, no dynamical transition occurs for the nematic phase, and the time dependence remains qualitatively the same throughout. We have checked numerically that our phase diagram applies also to other initial conditions as well. Our results remain valid for short-range interactions for times shorter than the quasiparticle energy relaxation time [16–18], set by the additional short-range terms, similarly to the BCS case. Similar ideas apply to a QBT in three dimensions (3D) [37], which is left for future study [38].

VIII. SUMMARY

We have studied the interplay of nematic and QAH orders around a 2D QBT point in the presence of long-range interactions. In equilibrium, nematic order occupies a significant portion of the phase diagram, and can even coexist with QAH through a third-order quantum phase transition, before giving way to QAH order via a second-order phase transition. After a quantum quench, the gapped QAH order behaves similarly to a BCS superconductor, and vanishes in the steady state for small final couplings. Surprisingly, the gapless nematic order survives any quenches and remains finite in the steady state, due to the peculiar topology of the QBT, and defying the usual reasoning based on energetics.

ACKNOWLEDGMENTS

B.D. is supported by the Hungarian Scientific Research Fund No. K101244, No. K105149, No. K108676, and No. K199442, and by the Bolyai Program of the HAS. I.F.H. is supported by the NSERC of Canada.

APPENDIX: LONG-RANGE INTERACTION IN BOTH REAL AND MOMENTUM SPACE

The infinitely long-range interaction term,

$$H_{\rm int} = -\sum_{i=x,y,z} \frac{g_i}{4N} \left(\sum_{\mathbf{p}} S^i_{\mathbf{p}} \right)^2, \tag{A1}$$

also describes an infinitely long-range interaction in real space. $S^i_{\mathbf{p}} = \Psi^+_{\mathbf{p}} \sigma_i \Psi_{\mathbf{p}}$ is the analog of Anderson's pseudospin operator [29] with $\Psi^+_{\mathbf{p}} = (a^+_{\mathbf{p}}, b^+_{\mathbf{p}})$ and *not* the $\mathbf{p}$th Fourier component of the spin operator. First, we Fourier transform the field operators to real space as

$$\Psi^+_{\mathbf{p}} = \frac{1}{\sqrt{N}} \sum_{\mathbf{r}} \Psi^+_{\mathbf{r}} \exp(i\mathbf{rp}), \tag{A2}$$

with $\Psi^+_{\mathbf{r}} = (a^+_{\mathbf{r}}, b^+_{\mathbf{r}})$, where $a^+_{\mathbf{r}}$ and $b^+_{\mathbf{r}}$ are creation operators of electrons in the $\mathbf{r}$th unit cell on the two distinct sublattices, respectively. Using this, we obtain

$$\begin{aligned} \sum_{\mathbf{p}} S^i_{\mathbf{p}} &= \frac{1}{N} \sum_{\mathbf{r},\mathbf{r}',\mathbf{p}} \Psi^+_{\mathbf{r}} \sigma_i \Psi_{\mathbf{r}'} \exp[i\mathbf{p}(\mathbf{r}-\mathbf{r}')] \\ &= \sum_{\mathbf{r},\mathbf{r}'} \Psi^+_{\mathbf{r}} \sigma_i \Psi_{\mathbf{r}'} \delta_{\mathbf{r},\mathbf{r}'} = \sum_{\mathbf{r}} \Psi^+_{\mathbf{r}} \sigma_i \Psi_{\mathbf{r}} = \sum_{\mathbf{r}} \mathcal{S}^i_{\mathbf{r}}, \end{aligned} \tag{A3}$$

where $\mathcal{S}^i_{\mathbf{r}} = \Psi^+_{\mathbf{r}} \sigma_i \Psi_{\mathbf{r}}$ is the pseudospin operator in the $\mathbf{r}$th unit cell. This yields an infinitely long-range interaction between the pseudospins in real space as

$$\begin{aligned} H_{\rm int} &= -\sum_{i=x,y,z} \frac{g_i}{4N} \left(\sum_{\mathbf{r}} \mathcal{S}^i_{\mathbf{r}} \right)^2 \\ &= -\sum_{i=x,y,z} \frac{g_i}{4N} \sum_{\mathbf{r},\mathbf{r}'} \mathcal{S}^i_{\mathbf{r}} \mathcal{S}^i_{\mathbf{r}'}. \end{aligned} \tag{A4}$$

[1] J. Dziarmaga, Adv. Phys. **59**, 1063 (2010).
[2] A. Polkovnikov, K. Sengupta, A. Silva, and M. Vengalattore, Rev. Mod. Phys. **83**, 863 (2011).
[3] J. Cayssol, B. Dóra, F. Simon, and R. Moessner, Phys. Status Solidi RRL **7**, 101 (2013).
[4] N. H. Lindner, G. Refael, and V. Galitski, Nat. Phys. **7**, 490 (2011).
[5] M. S. Foster, V. Gurarie, M. Dzero, and E. A. Yuzbashyan, Phys. Rev. Lett. **113**, 076403 (2014).
[6] J. Dukelsky, S. Pittel, and G. Sierra, Rev. Mod. Phys. **76**, 643 (2004).
[7] G. Ortiz, J. Dukelsky, E. Cobanera, C. Esebbag, and C. Beenakker, Phys. Rev. Lett. **113**, 267002 (2014).
[8] M. F. Maghrebi, Z.-X. Gong, and A. V. Gorshkov, arXiv:1510.01325.
[9] D. Loss, F. L. Pedrocchi, and A. J. Leggett, Phys. Rev. Lett. **107**, 107201 (2011).
[10] R. Mottl, F. Brennecke, K. Baumann, R. Landig, T. Donner, and T. Esslinger, Science **336**, 1570 (2012).
[11] C. Maschler, I. B. Mekhov, and H. Ritsch, Eur. Phys. J. D **46**, 545 (2008).
[12] F. Piazza and P. Strack, Phys. Rev. Lett. **112**, 143003 (2014).
[13] R. Landig, L. Hruby, N. Dogra, M. Landini, R. Mottl, T. Donner, and T. Esslinger, Nature (London) **532**, 476 (2016).
[14] D. Porras and J. I. Cirac, Phys. Rev. Lett. **92**, 207901 (2004).
[15] J. W. Britton, B. C. Sawyer, A. C. Keith, C.-C. J. Wang, J. K. Freericks, H. Uys, M. J. Biercuk, and J. J. Bollinger, Nature (London) **484**, 489 (2012).
[16] R. A. Barankov, L. S. Levitov, and B. Z. Spivak, Phys. Rev. Lett. **93**, 160401 (2004).
[17] R. A. Barankov and L. S. Levitov, Phys. Rev. Lett. **96**, 230403 (2006).
[18] E. A. Yuzbashyan and M. Dzero, Phys. Rev. Lett. **96**, 230404 (2006).
[19] E. A. Yuzbashyan, O. Tsyplyatyev, and B. L. Altshuler, Phys. Rev. Lett. **96**, 097005 (2006).
[20] A. Faribault, P. Calabrese, and J.-S. Caux, J. Math. Phys. **50**, 095212 (2009).
[21] A. Moor, P. A. Volkov, A. F. Volkov, and K. B. Efetov, Phys. Rev. B **90**, 024511 (2014).
[22] W. Fu, L.-Y. Hung, and S. Sachdev, Phys. Rev. B **90**, 024506 (2014).

[23] M. Dzero, M. Khodas, and A. Levchenko, Phys. Rev. B **91**, 214505 (2015).
[24] K. Sun, H. Yao, E. Fradkin, and S. A. Kivelson, Phys. Rev. Lett. **103**, 046811 (2009).
[25] O. Vafek and K. Yang, Phys. Rev. B **81**, 041401 (2010).
[26] R. Nandkishore and L. Levitov, Phys. Rev. B **82**, 115124 (2010).
[27] B. Dóra, I. F. Herbut, and R. Moessner, Phys. Rev. B **90**, 045310 (2014).
[28] M. Z. Hasan and C. L. Kane, Rev. Mod. Phys. **82**, 3045 (2010).
[29] P. W. Anderson, Phys. Rev. **112**, 1900 (1958).
[30] K. Novoselov, E. McCann, S. Morozov, V. Falko, M. Katsnelson, U. Zeitler, D. Jiang, F. Schedin, and A. Geim, Nat. Phys. **2**, 177 (2006).
[31] S. Sorella and E. Tosatti, Europhys. Lett. **19**, 699 (1992).
[32] B. Sciolla and G. Biroli, J. Stat. Mech.: Theory Exp. (2011) P11003.
[33] F. Peronaci, M. Schiró, and M. Capone, Phys. Rev. Lett. **115**, 257001 (2015).
[34] V. Gurarie, Phys. Rev. Lett. **103**, 075301 (2009).
[35] A. H. Castro Neto, F. Guinea, N. M. R. Peres, K. S. Novoselov, and A. K. Geim, Rev. Mod. Phys. **81**, 109 (2009).
[36] H. Won and K. Maki, Phys. Rev. B **49**, 1397 (1994).
[37] J. M. Luttinger, Phys. Rev. **102**, 1030 (1956).
[38] A QBT in 3D is unstable with respect to ordering in five different channels [39,40]. Depending on the anisotropy of the long-range interaction, several ordered configurations are expected to be realized and the quench dynamics would be sensitive to the symmetry and topology of the ordering.
[39] I. F. Herbut and L. Janssen, Phys. Rev. Lett. **113**, 106401 (2014).
[40] L. Janssen and I. F. Herbut, Phys. Rev. B **92**, 045117 (2015).